Low-cost, multimodal environmental monitoring based on the Internet of Things

Graham Coulby[a]; Adrian K. Clear[b]; Oliver Jones[c]; Alan Godfrey[a,*];

[a] Department of Computer and Information Sciences, Faculty of Engineering and Environment, Northumbria University, Newcastle Upon Tyne, NE1 8ST (e-mail: g.d.coulby@northumbria.ac.uk; a.godfrey@northumbria.ac.uk)
[b] School of Computer Science, College of Science and Engineering, National University of Ireland Galway, Galway, Ireland. (email: adrian.clear@nuigalway.ie)
[c] O. Jones is the Director of Research, Ryder Architecture, Newcastle Upon Tyne, NE1 3NN (e-mail: ojones@ryderarchitecture.com)

ARTICLE INFO

Keywords:
Indoor Environmental Quality *(IEQ)*
Sensor Fusion
Multimodal
Internet of Things (IoT)
Building Performance

Monitoring Indoor Environmental Quality (IEQ) is of growing interest for health and wellbeing. New building standards, climate targets and adoption of homeworking strategies are creating needs for scalable, monitoring solutions with onward Cloud connectivity. Low-cost Micro-Electromechanical Systems (MEMS) sensors have potential to address these needs, enabling development of bespoke multimodal devices. Here, we present insights into the development of a MEMS-based Internet of things (IoT) enabled multimodal device for IEQ monitoring. A study was conducted to establish the inter-device variability and validity to reference standard sensors/devices. For the multimodal, IEQ monitor, intraclass correlations and Bland-Altman analyses indicated good inter-sensor reliability and good-to-excellent agreement for most sensors. All low-cost sensors were found to respond to environmental changes. Many sensors reported low accuracy but high precision meaning they could be calibrated against reference sensors to increase accuracy. The multimodal device developed here was identified as being fit-for-purpose, providing general indicators of environmental changes for continuous IEQ monitoring.

1 Introduction

Monitoring Indoor Environmental Quality (IEQ) is critically important, due to the amount of time people spend indoors [1]. Concerns surrounding inadequate IEQ are resulting in increased number of green building standards designed around health and wellbeing metrics [2]. To achieve these standards, there is a need to monitor indoor environments (as well as the health and wellbeing of building occupants). However, monitoring equipment can be complex and costly, acting as a barrier by reducing feasibility of monitoring solutions beyond research [3]. Additionally, the 2019 SARS-COV-2 pandemic has been a catalyst to hasten need for pragmatic remote healthcare monitoring in enclosed spaces, where previous suggestions have been unpopular [4].

The dominant approach to monitoring IEQ is with research grade devices, which offer excellent quality data but have many limitations. They are often unimodal, measure only one aspect of IEQ and can cost thousands of US dollars [3]. Given that IEQ is determined by many different factors, this requires multiple devices to gain a holistic picture.. Consequently, indoor spaces are often measured from a single location, reducing the spatial density of IEQ measurements [5], [6], limiting what can be inferred about the health and wellbeing of a spatially distributed set of occupants. Research grade devices can be moved between locations, but this limits long-term measurements in any one location, meaning data from different locations will not be temporally comparable.

Occasionally it may be beneficial to sacrifice precision and accuracy of measurement for gains in spatial density and longitudinal monitoring. Low-cost sensor technologies could positively impact on building sciences (and the wider healthcare, architecture, engineering and construction fields), as they enable multimodal monitoring devices that can measure a range of IEQ factors from a single low-cost device [1]. Thus, low-cost sensors would be a likely requirement in creating devices that could be scalable to support localised and therefore, increased spatial dense IEQ monitoring. Such devices could capture remote longitudinal IEQ data in many locations, providing greater insights into the long-term effects of indoor environments on occupants [7].

Individualised occupant health and wellbeing could also be assessed by identifying patterns in localised, longitudinal data [8]. Localised sensors could provide occupants with guidance on how they can self-manage their comfort by *e.g.*, recommending a different location that has environmental conditions closer to their preferences.

Lack of Cloud connectivity is another limitation with many research grade monitoring devices, where IEQ data is recorded to internal storage, which removes the possibility of accessing real-time data [3]. Low-cost sensor technologies

could address this limitation as many processing units that control low-cost sensors are IoT enabled, reading and writing data to the Cloud in real-time [1] and enabling data to be analysed while devices are deployed.

While low-cost technologies are enabling the development of pragmatic and affordable solutions for remote monitoring, there is a general lack of acceptance towards low-cost sensor technologies [3]. This issue is further complicated by a lack of transparency from manufacturers of consumer-grade monitoring equipment, that utilise low-cost sensors. While manufacturers typically publish accuracy information and technical specifications they often negate to publish which sensors are used in their devices, which results in the need to explore internal photographs from Federal Communications Commission (FCC) reports or dismantle devices to identify sensors [9]. This means there are requirements to continually benchmark, verify and validate these technologies to reference (gold) standard devices. This can be extremely costly and impracticable to implement [9]–[13].

Here, the primary aim is to investigate and develop a multimodal, IoT-enabled, monitoring device that is low-cost and scalable, to support localised environmental monitoring. A secondary aim is to compare the accuracy and precision of the low-cost sensors with reference standard devices, used in IEQ research, to determine suitability of low-cost sensors for applications in this space. The multimodal approach is constructed to measure a wide range of important IEQ factors.

2 Related work

Air quality, thermal comfort, sound/noise and light are the four most commonly measured factors of IEQ [14], [15]. Low-cost sensors can be used to measure a range of data relating to those factors, but differences exist in the technologies and methods used to derive them [3]. This section will provide a rationale for the selection of low-cost sensors in the proposed multimodal device by comparing and contrasting to reference standards.

2.1 Inclusion criteria: Sensor integration

Cost and accessibility of IoT technology has resulted in a vast array of instruments. Many have a great deal of support *(manufacturers and the IoT community of users [1])* where, e.g., hardware is supported by official code-libraries to expedite integration between sensors and microcontrollers [16]. Many libraries provide mechanisms to read and process sensor data, with minimal coding. In addition to low-cost, availability of libraries and functionality within was another inclusion factor within this study when selecting low-cost sensing instrument.

2.2 Low-cost IEQ sensing

Air quality: equivalent Carbon Dioxide (eCO_2) and Volatile Organic Compounds (VOCs)

Non-dispersal, infra-red (NDIR) sensors are most commonly used as the reference/gold standard for measuring Carbon Dioxide (CO_2) [17]. However, sensors that measure eCO_2 *(known as equivalent or estimated CO_2)* are becoming more popular due to their low-cost (*approx US$5-10)* [1]. Yet eCO2 sensors are often used in place of CO_2 sensors and incorrectly reported as CO_2 [18]–[20].

eCO_2 sensors use a heated Metal Oxide (MOx) semiconductor on which oxygen reacts with gasses to change the resistance, proportional to gas concentrations [21]. However, MOx sensors are highly sensitive to environmental conditions and a wide range of gases and pollutants, which can have a major influence on measurement accuracy [22]. As the name suggests, eCO_2 is not an actual measure of carbon dioxide but an estimation. The value is derived from a measurement of the Total VOCs (TVOCs), which describe the total concentration of organic, carbon-based compounds that evaporate into the air at room temperature [23]. There is a lack of clarity around what TVOC sensors actually measure and also little information about how the readings are calculated or whether readings/outcomes are standardised [24]–[26]. Algorithms that estimate TVOC values are typically implemented within the on-board microcontroller of the sensors and are often black boxed [3]. General assumptions are also made during the calculation of both TVOC and eCO_2. For example, TVOC sensors assume the primary source of VOC is from humans and validity can be questioned when measuring in environments where this is not case [24].

Naepelt [27] provided transparent algorithms for eCO_2/TVOC calculations, but they depend on knowing the proportion of human generated VOCs. For their calculations, they assert that human generated VOCs increase gradually, and VOCs released from aerosols or cooking increase rapidly. However, TVOCs are most commonly released by finishes and furnishings, especially those made using artificial materials such as solvents and adhesives [28]. As room temperature affects the concentration of such VOCs [23], it cannot be assumed that all artificial VOCs increase TVOC concentrations rapidly. Moreover, there can potentially be hundreds of VOCs within indoor air [29], so making assumptions based on one or two of the most volatile compounds is likely to have inaccuracies.

Given the limitations of TVOC sensors, they will not be used as a measure of air quality in the proposed multimodal device. However, since eCO_2 is often misrepresented as a measurement of CO_2 [18]–[20], a MOx eCO_2 sensor was selected for comparing eCO_2 readings with readings from reference CO_2 sensors. This was to identify whether eCO_2 readings have any correlation with CO_2 concentrations and to understand whether it is suitable to use them in place of NDIR CO_2 sensors. Thus, an AMS CCS811 *(Table 1)* was selected for our multimodal device as it is regarded as a reliable solution for measuring gas concentrations [30]–[32]. Consequently, a CCS811 breakout board was chosen as it provides an I^2C interface and is supported by an official Adafruit Arduino code library [33].

Air quality: Carbon Dioxide (CO_2)

High concentrations of CO_2 can have a range of impacts on productivity and cognitive performance [34], It is therefore often used in work place IEQ studies. However, extremely high concentrations of CO_2 are required before it becomes detrimental to health [34]. Thus, CO_2 is often regarded as a poor indicator of Indoor Air Quality (IAQ) [35]–[37]. Nevertheless, it has become more commonly used in IAQ/IEQ monitoring as a proxy outcome for ventilation [37], [38]. Focus on CO_2 sensors for ventilation monitoring has increased rapidly since the outbreak of the SAR-COV-2 pandemic [39], [40], to monitor the circulation of fresh air within buildings and to help stop the spread of the virus. This greatly increases their importance in IEQ monitoring and provides a need for monitoring solutions that can be deployed at scale.

NDIR sensors set the standard for CO_2 measurements [17] and technological advancements are driving a growing market of low-cost sensors that can also measure CO_2 using the same NDIR technology [41]. Due to the complexity of NDIR components, even the lowest costing NDIR sensors (approx. US$20) is greater than the cost of most MOx sensors. However, the price range of low-cost NDIR CO_2 sensors is much broader than MOx sensors. For example, a previous study [3] identified several low-cost, NDIR CO_2 sensors that ranged from US$20 (MH-Z19, Winsen Electronics) to US$200 (CozIR, Gas Sensing Solutions), with most costing approx. US$100. Here, the MH-Z19 (Table 1) was the most viable option for use in the proposed multimodal device. Despite its low cost, the MH-Z19 is regarded as a reliable, stable and accurate sensor for CO_2 measurement [42]–[44]. The MH-Z19 is supported by Dempsey's Arduino library [45], which provides many functions for interfacing. Air quality: Particulate matter (e.g., $PM_{2.5}$)

$PM_{2.5}$ is used to describe airborne particulate matter. The '2.5' refers to particles that are up to 2.5µm *(microns)* in diameter. The term PM_{10} is also used to describe particles >2.5 microns, but <=10 microns. $PM_{1.0}$ is used to describe the smallest range of particles (up to 1.0 microns), but is not standardised by global environmental protection agencies (EPAs) [46]. The current specification of the US EPA is that within no 24-hour period should $PM_{2.5}$ exceed 35µg/m^3 [47].

Measurement of particulates and the pollutants within them requires expensive equipment that collects particles in a filter and measures the weight increase using a Tapered Element Oscillating Microbalance (TEOM) [48]. Lower-cost, optical, sensing technologies can also be used to measure PM, but these cannot detect particles <0.25µm and can miss some sources of pollution such as a cooking that does not involve frying or heating oil [48].

A previous review [9] identified the scientific potential of the FooBot Air Quality monitor, which uses a Sharp GP2Y1010AU0F (GP2YX) optical dust sensor [9]. Therefore, the GP2YX was selected for use in the low-cost multimodal device, but initial testing with the GP2YX produced erratic and highly inaccurate data. Alternatively, PlanTower sensors are often used in many commercial devices [48] and have been found to report data that correlates with reference equipment when measuring $PM_{2.5}$ [49]–[51]. Therefore, a (PlanTower) PMSA003 *(Table 1)* sensor was selected here to measure $PM_{2.5}$. The Adafruit PMSA003i variant of the sensor was chosen as it provides an I^2C interface and an official Arduino code library to interact with the sensor [52].

Thermal comfort: Temperature and humidity

Temperature and humidity have an influential role in IEQ monitoring as optical sensors that detect airborne particles and molecules (such as those used to measure CO_2 and PM) can be highly impacted by thermal changes [53]. Therefore, many commercial devices include a temperature and humidity sensor to support and/or calibrate the primary sensors [3].

Hygrometers are commonly used to measure humidity and temperature simultaneously. Hygrometers are typically small *(approx. 1cm^2)*, low-cost *(approx. $2-5)* devices that output signals which can be read by analogue inputs on microcontrollers and processed with an Analogue-to-Digital Convertor (ADC). MEMS technologies are also used to measure temperature and humidity, providing a range of benefits over traditional hygrometers. For example, they are significantly smaller than analogue hygrometers *(approx. 2mm^2)* and have integrated amplification and ADC circuitry.

Given the role temperature and humidity play on other sensor technologies, there are a plethora of low-cost sensors. However, the Bosch BME280 *(Table 1)* sensor was chosen as it is a low-cost, multimodal, MEMS sensor that is used within healthcare applications [54]. Moreover, the sensor also captures barometric air pressure, which can also impact readings from optical sensors [53]. A BME280 breakout board was chosen as it provides an I^2C interface and is supported by an official Adafruit Arduino code library [55].

Light: Ambient light intensity

Light intensity can be a source of discomfort for occupants, causing distractions, eye pain and skin conditions [56]. There are two common approaches for measuring light intensity *(in lux):* (i) Light Dependant Resistor (LDR), that reduces the resistance across a circuit as light intensity increases [57] and (ii) photodiodes, which converts light intensity into an electrical current [58]. LDRs have a response delay between light exposure and resistance decrease, which can be a limitation in high frequency measurement [58]. Photodiodes can use filters to target specific frequencies bands in a light spectrum and can obtain more precise measurements across a broader range of light intensities compared to LDRs [59]. They are often incorporated into integrated circuits that contain amplification circuitry and an ADC [60]. This can provide more control of the output measurements. Previous work examined the *ROHM BH1750* photodiode sensor *(Table 1)* [1], where it was found to be highly correlative to research standard sensors. Thus, it was selected here for the

multimodal device. The BH1750 is also available as an I^2C breakout board and was setup according to the installation instructions and code libraries provided with the sensor [61].

Sound/noise: Noise levels

Microphones work by converting sound pressure into a linear electrical signal, meaning the latter directly correlates with the sound signal [62]. To measure loudness, decibels (dB) logarithmically scale to mirror human hearing sensitivity [63], [64]. Therefore, to measure dBs with a microphone, the output voltage from microphones is converted to the logarithmic dB scale. The complexity of the logarithmic calculation is highly dependent on the sensitivity of the microphone. Yet how the sensitivity of a microphone is determined is influenced by the selection of an analogue or a digital microphone.

The voltage of analogue microphones typically needs to be routed through both a pre-amp and an audio codec that converts the analogue signal to digital using an ADC [65]. This three-stage approach can be affected by other circuitry and communication signals such as Wi-Fi and Bluetooth [66]. Therefore, it is often appropriate to use digital microphones, built using MEMS, as they have an in-built ADC that converts the signal directly from the microphone and is therefore not as susceptible to circuit noise [66].

Since the microphone within the proposed multimodal device will be housed in close proximity to the microcontroller *(WiFi and Bluetooth enabled)*, a digital MEMS microphone was selected to minimise interference [66]. The InvenSense INMP441 *(Table 1)* microphone was chosen here, which is supported by Kostoski's ESP32 library for I^2S digital microphones [67]. This library is specifically designed for digital MEMS microphones and calculates A-weighted decibel readings from MEMS microphones and provides the necessary filters and equalisation to do so, which are based on precalculated analyses conducted in MATLAB®.

Table 1 – Low-Cost sensors used for development including min/max measurement thresholds and units that are measured

Measure	**Instrument**[†]	**Protocol**	**Cost**[‡]	Min	Max
TVOC (ppb) eCO2 (ppm)	**CCS-811** [24]	I^2C	$5	0 400	1187 8192
CO_2 (ppm)	**MH-Z19B**[§] [68]	UART PWM DAC	$20	0 0	2000 5000
$PM_{2.5}$ (µg/m^3)	**PMSA003i** [69]	I^2C	$16	0	500
Temp (°C) Humidity (%) Pressure (hPa)	**BME280** [70]	I^2C	$2	-40 0 300	85 100 1100
Light (lux)	**BH1750** [71]	I^2C	$1	1	65535
Noise (dB SPL)	**INMP441** [72]	I^2S	$2	33	120

[†] Detailed technical specifications for each sensor (including voltage requirements, accuracies and working temperature/humidity) can be found within the referenced datasheets; [‡] All prices (rounded to the nearest USD) are taken from AliExpress.com (10 November 2020).; [§] The MH-Z19B supports two measurement ranges (0-2000ppm and 0-5000ppm) over the UART protocol only.

2.3 Cloud connectivity

IoT cloud computing is largely dominated by Amazon, Google and Microsoft [73], but there are hundreds more readily *(low-cost/free)* accessible platforms, many tailored for unique use cases [74]. Many IoT platforms provide free but limited functionality for testing and prototyping. Equally there are often hidden costs with these services that need to be considered before choosing platforms for production [1].

Previously, ThingSpeak® [1] was identified as a fit-for-purpose IoT/Cloud platform when conducting IEQ monitoring. It is developed by the creators of MATLAB® and supports real-time transmission and visualisations of data from IoT devices and if required, Cloud-based analysis using MATLAB® code [1]. For the purposes of this study, the quota provided in the free package was enough to evaluate the feasibility of real-time transmission from the prototype, without any costs. ThingSpeak® also provides an official code library to transmit data from various microcontrollers to the Cloud. This meant that a simple interface could be created to encapsulate the data transmission function of the code library, meaning that ThingSpeak® could be easily switched out to different IoT platforms, if required.

3 Reference devices

3.1 Onset HOBO® MX1102 (CO_2 and eCO_2)

The HOBO® MX1102 *(Table 2)* datalogger was selected to measure CO_2 due to high accuracy at room temperature [75], [76]. Although not an IoT device, it has a large storage capacity and is able to gather data continuously for several months. Since eCO_2 sensors will also be included in the multimodal device, to evaluate the validity of eCO_2 readings, the HOBO® MX-1102 sensor was also used as a reference for eCO_2 readings.

3.2 IQAir Air Visual Pro ($PM_{2.5}$)

Due to cost and complexity of reference standard PM monitoring equipment, where single units can cost several thousands of dollars [3], it was not possible to obtain a true reference within the budget of this study. However, a previous study [48] evaluated several lower-cost monitors *(defined as devices <US$300)*, concluding that those lower-cost monitors may be used to efficiently detect $PM_{2.5}$ events. In that study, the validity of six low-cost, optical $PM_{2.5}$ were examined against a TEOM, which measured the actual mass of dust particles. Of the sensors examined, two were available at the time of the study *(Kaiterra: Laser Egg 2 and IQAir: Air Visual Pro).* The ratio of both device measurements against the TEOM was ≤1:2 but for most test events the IQAir Air Visual Pro (AVP) reported closer to the true mass concentrations captured by the TEOM. Additionally, IQAir calibrate each device against a Grimm 11-A [48] sensor, which is commonly used as a research standard measure of $PM_{2.5}$ [77]–[79]. Based on these findings, the AVP *(Table 2)* was selected as a $PM_{2.5}$ reference for this study.

3.3 Onset HOBO® MX1104 (Light intensity, temperature, humidity)

An Onset HOBO® datalogger was also used as a reference standard to measure ambient light intensity. The MX1104 *(Table 2)* features a similar interface to the MX1102 but measures light intensity alongside temperature and humidity. Like the MX1102, the MX1104 has large internal storage and is also highly accurate at room temperature. Temperature and humidity were validated against the HOBO® MX1104 as both HOBO® devices measure these factors, but (*according to the manufacturer's specifications)* the MX1104 has a slightly higher accuracy for temperature and humidity than the MX1102.

3.4 Air Pressure

To validate results from the BME280's air pressure sensor, data were compared to outdoor air pressure extracted from the weather.com API. The following endpoint was used to acquire data from the study location (Newcastle Upon Tyne, UK) during the sample period:

https://api.weather.com/v1/location/EGNT:9:GB/observations/historical.json?apiKey=<API_KEY>&units=m&startDate=20201101&endDate=20201130.

3.5 Omega HHSL-101 (noise levels)

The Omega HHSL-101 *(Table 2)* sound level meter was selected as it has a similar dynamic range *(100dB SPL)* to the INMP441 *(87dB).* Many sound level meters are designed for real-time measurements, but to validate the INMP411 it was important that data could be logged, extracted and analysed. The Omega HHSL-101 logs with a decimal resolution *(0.1dB)* to internal storage, up to 32,000 samples. At 10 second (s) intervals, this is not a large amount of storage, but it enables data capture to run a comparative analysis.

Table 2 – Reference devices used, with indicative costs, min/max measurement thresholds and units

Measure	Instrument†	Cost‡	Min	Max	Units
CO_2 (ppm)	**Onset**		0	5000	ppm
Temp (°C)	**HOBO®**	$595	0	50	°C
Humidity (%)	**MX-1102** [80]		1	70	%
Light (lux)	**Onset**		0	167,731	lx
Temp (°C)	**HOBO®**	$185	-20	70	°C
Humidity (%)	**MX-1104** [81]		0	100	%
$PM_{2.5}$ (µg/m³)			0	1,798	µg/m³
CO_2 (ppm)	**IQAir Air Visual Pro** [82]	$269	400	10,000	ppm
Temp (°C)			-10	40	°C
Humidity (%)			0	95	%
Noise (dB SPL)	**Omega HHSL-101** [83]	$149	30	130	dB SPL

† Detailed technical specifications for each sensor (including voltage requirements, accuracies and working temperature/humidity) can be found within the referenced datasheets; ‡ All prices (rounded to the nearest USD) are taken from the manufacturer's websites via Google Shopping - with the region set to United States (10 November 2020).

4 Multimodal device architecture

4.1 Hardware development

For testing, three multimodal devices were constructed to test low-cost devices/sensors against reference standards, and to test inter-sensor reliability. The low-cost sensors were connected to a Heltec Wi-Fi Kit 32 ESP32 microcontroller on

a solderless breadboard (Figure 1). Additional schematic diagrams and detailed breadboard configurations have also been included in the supplementary material.

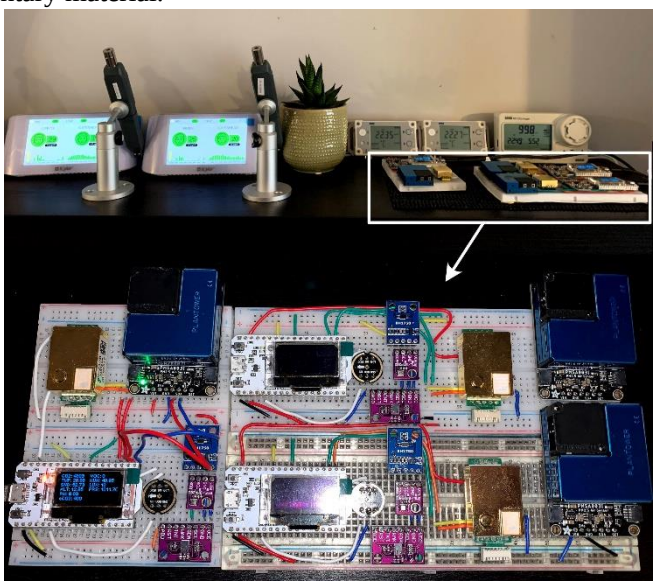

Figure 1 - Low-cost sensors collecting data alongside reference devices. Including a closeup image to show the breadboard configuration.

The Heltec was selected as it included Wi-Fi for Cloud *(Figure 2)* communication and a built-in OLED display for real-time feedback. The specifications for the Heltec also made it a suitable choice for the intended application as the included communication interfaces *(3x UART; 2x I^2C; 1 x I^2S)* can support a simultaneous connection to all sensors. Despite its size, the Heltec also has 3V and 5V output, when powered with USB, meaning it can power the MH-Z19B without additional voltage boosting circuity.

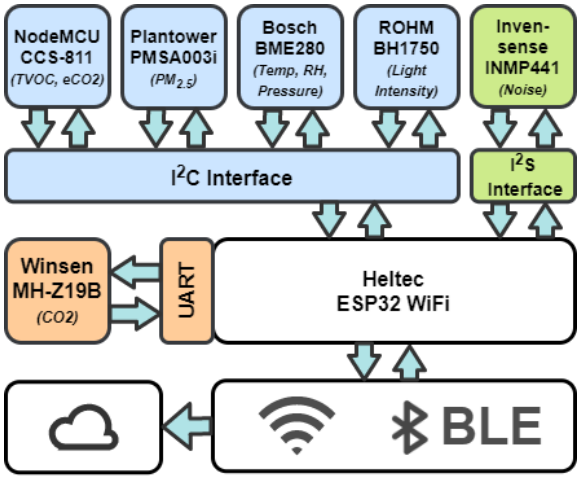

Figure 2 - Schematic diagram for multi-modal IEQ sensor device.

A mix of the Arduino IDE and Visual Studio Code (with the Arduino extension) were used to program the ESP32 with C++ code. The ESP32 can be programmed with both Arduino code and Micro Python code, but the Arduino workflow was chosen because of its maturity and wider support for sensors.

4.2 Reading CO_2 data via UART

The MH-Z19B outputs data via Pulse Wave Modulation (PWM) Digital Analogue Conversion (DAC) or Universal Asynchronous Receiver-Transmitter (UART). UART was selected as it enabled the read/write of byte commands to request and receive data, which facilitates a range of additional functionality, Table 3. These commands also allow the device to be configured to utilise the full measurement range of the sensor *(0-5000ppm).*

To read CO_2 data from the MH-Z19B a byte command is first sent to the sensor's microcontroller. After processing, the MH-Z19B sends data back to the requester as a return byte command. These commands will be sent as Byte3 when sending a command to the sensor and returned as Byte2 when receiving data from the sensor, Table 3.

Table 3 - MH-Z19B UART Commands

Action	Byte0	Byte1	Byte2	Byte3	Byte 4 – 7	Byte8
Send Command	0xFF	0x01	CMD†	0x00	0x00	0x79
Receive Command	Start	CMD†	High Level	Low Level	-	Check

† UART Byte commands available on the MHZ19B - **0x78:** Recovery Reset; **0x79:** ABC Mode ON/OFF; **0x84:** Raw CO2; **0x85:** Temp float; **0x86:** Temp integer; **0x87:** Zero Calibration; **0x88:** Span Calibration; **0x99:** Range; **0x9B:** Get Range; **0x9C:** Get Background CO2; **0xA0:** Get Firmware Version; **0xA2:** Get Last Response; **0xA3:** Get Temp Calibration.

The MH-Z19B uses Automatic Baseline Calibration (ABC), enabled by factory default, that calibrates 400pm to the lowest measured PPM in the last 24-Hour cycle. The sensor also supports zero-point calibration, whereby the sensor can be manually set to 400ppm. Manual calibration was done to all MH-Z19B sensors on the first connection, due to high initial output values. To do this, sensors were connected to a microcontroller and placed outdoors. After exposing the sensors to 400ppm for 20 minutes (mins), the zero-point calibration was set by connecting the **Hd** pin to **GND** on each sensor for approx. 7s.

4.3 Reading PM, temperature, humidity and ambient light intensity data via I^2C

Four sensors communicated with the microcontroller via an I^2C bus, Table 1. This was chosen because it is a serial communication protocol that uses a two-wire interface: (i) the Serial Data *(SDA)* wire sends data across the bus, and the (ii) Serial Clock *(SCL)* wire synchronises communication between the master (microcontroller) and slaves (sensors) [84]. As the protocol requires two wires only to form the serial bus, it is optimal in microcontroller applications. Thus, it has become standardised for ARM microcontrollers [85]. Moreover, the ability to read from multiple sensors from a single two-wire bus makes this protocol extremely useful for multimodal devices [86].

Each I^2C slave communicates on its own unique I^2C address. Some sensor manufacturers develop sensors with multiple I^2C buses to allow more than one of the same slaves to communicate with an I^2C master. Addresses for CCS811 and BH1750 can be changed with a software modification, typically by specifying the address, when declaring a new instance of sensor within a code library. However, the BME280 requires a hardware modification to switch addresses. On the front of the breakout board there are three solder points (i.e. jumpers). If no jumpers are joined, *(or the two left-most jumpers are joined)* the device defaults to address 0x76. However, if the two right-most jumpers are soldered the address is changed to 0x77. I^2C multiplexors can also be used which have separate busses for communicating with sensors. Each bus works the same way as the I^2C bus on an MCU, in that multiple devices can be connected if there are no address conflicts. However, each bus of the multiplexor has its own access address and each bus is separated from one another [87]. This means that address conflicts can be resolved by connected devices with conflicts to separate busses. For this study, there were no I^2C address conflicts in the multimodal device. Consequently, multiplexors were not required and the default addresses for each sensor were used.

4.4 Reading noise data via I^2S

To calculate the Sound Pressure Level (SPL) in dB with a microphone, a logarithmic calculation is required:

$$dB = 20 \times log_{10}\left(\frac{S_{RMS}}{ref}\right) \qquad (1)$$

Where S_{RMS} is the root mean squared of the samples captured by the microphone over a given sample period *(*e.g., *1000ms)* and *ref* is the peak amplitude of the microphone. To calculate $S_{RMS,}$ Kostoski's library first applies equalisation and filtering to the samples and calculates the sum of squared, weighted samples:

$$S_w = \sum_{0}^{N} y^2 \qquad (2)$$

Where *N* is the number of samples captured in the sample period and *y* is the samples after weighting and equalisation have been applied. The sum of samples is then used to calculate the S_{RMS}:

$$S_{RMS} = \sqrt{\frac{S_w}{N}} \qquad (3)$$

To calculate the peak amplitude *(ref*, Eq. 1*)* the sensitivity of the microphone must first be calculated. For digital microphones, the sensitivity of the microphone should be pre-specified in the microphone's datasheet and is calculated as:

$$Sens_{dBFS} = dB_{REF} - dB_{MAX} \qquad (4)$$

Where dB_{REF} is 94dB *(equivalent to 1 Pascal)*, and dB_{MAX} is the maximum acoustic input for the given microphone. For the INMP441, the specified maximum acoustic input is 120dB (Table 1) so the resulting sensitivity is -26dBFS.

Once sensitivity is calculated, it is then used to calculate the peak amplitude of the microphone that is used as the *ref*, *Eq* (1). The INMP441 datasheet [72] specifies that the peak amplitude for this microphone is calculated as:

$$ref = \left(2^{(bitrate-1)} - 1\right) \times \left(10^{(dBFS/20)}\right) \qquad (5)$$

Since the INMP441 transmits data via a 24-bit I^2S interface [72], the peak amplitude of the microphone therefore maps to 420,426 discreet digital values.

5 Methods

5.1 Data acquisition and connectivity

All data from low-cost sensors were read and processed by a HELTEC ESP32 Wi-Fi microcontroller (a dual-core microcontroller with Wi-Fi, Bluetooth, Bluetooth Low Energy (BLE) and an integrated Liquid Crystal Display (LCD) display). A reading for each sensor was collected every 15s and data were written to ThingSpeak®, which allows up to eight sensor readings *(per channel)* to be written to the Cloud simultaneously. The data/channel quota included with a free subscription was suitable to test the prototype and conduct validation of sensors in each device.

5.2 Data processing

The intervals between measurements, for each device (low-cost and reference), were determined from when the devices were initially configured to initiate logging. Therefore, it was not possible to synchronise the sample rate across devices. Consequently, there was a need to resample data extracted from the measurement instruments to ensure they were comparable. A series of steps were undertaken for data processing and analysis (Figure 3).

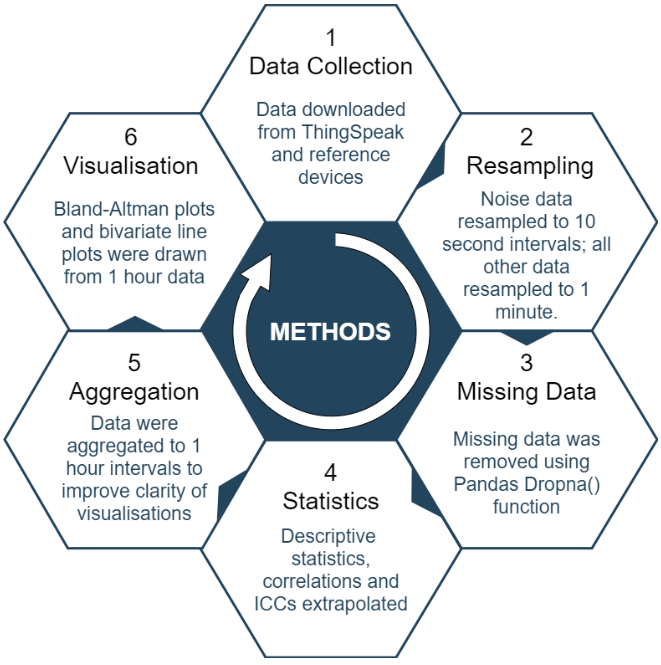

Figure 3 - Data processing methods

Resampling (excluding noise level data)

A sample rate of 1min was chosen for resampling to reduce the amount of interpolated data in the final dataset. Since the sample rate of the reference standard sensors was 5mins this meant up-sampling all reference standard sensors by

interpolating the values for the missing intervals. This was done using the pre-processing package from the Sci-Kit Learn library for Python, using a linear interpolation method. Conversely, down-sampling was required to resample sensor data from low-cost sensors, which captured sensor readings with a 15s sample rate. Sci-Kit Learn was also used to resample those data, but the mean function was used on the data series to calculate the mean for each 1min period.

Missing data

After resampling data, the rows which contained missing data were dropped using the Pandas' Dropna function so that a bivariate analysis could be performed on any two columns without conflicts. A dataset was created that contained a total of 15,828 samples. Those data were combined into a single Pandas DataFrame for processing. (Since there were many gaps in the HHSL-101 data, due to the three-day reconfiguration cycle, noise data from the HHSL-101 and INMP441 were not included here).

Noise level data

INMP441 data were combined with HHSL-101 data separately using the same methods used for other sensors. Data were resampled with a 10s sample rate and the resulting dataset contained 47,602 samples that were also combined into a single DataFrame.

Analytical and statistical procedures

To analyse both data sets, Pandas was used in conjunction with Matplotlib, Seaborn, Sci-Kit Learn, Pingouin and the Statsmodel API libraries for Python. Pandas was used to provide descriptive statistics and to process datasets

Table 4 - Results of sensor validation study

Src	Dev†	Descriptive Statistics					P'son Corr	Agreement (Bland-Altman)			ICC§	
		Mean	Std	50%	75%	Max		Mean Dif	Std	LoA‡	$ICC_{2,1}$	$ICC_{3,1}$
eCO_2 (ppm) CCS811	ESP_A_eCO2	652.01	353.28	552.88	727.5	7899	0.38	-50.87	244.54	479.29	0.79 *[0.49 - 0.9]*	0.89 *[0.88 0.89]*
	ESP_B_eCO2	932.83	549.25	769.33	1052.38	7992	0.38	268.57	474.5	930.01		
	ESP_C_eCO2	964.95	520.06	779	1077.38	7632.75	0.36	311.39	456.52	894.79		
	Ref: MX1102	700.43	178.35	678.7	866.8	999	-	-	-	-		
CO_2 (ppm) MH-Z19	ESP_A_CO2	574.03	132.13	564	693	1260	0.97	-138.86	66	129.36	0.72 *[0.1 - 0.9]*	0.95 *[0.95 - 0.96]*
	ESP_B_CO2	748.38	144.28	743	873.75	1485.67	0.95	39.22	64.64	126.7		
	ESP_C_CO2	632.84	185.49	617.67	793.25	1611	0.96	-67.52	48.77	95.58		
	Ref: MX1102	700.43	178.35	678.7	866.8	999	-	-	-	-		
$PM_{2.5}$ (µg/m3) PMSA003i	ESP_A_PM25	4.92	17.19	0.00	2.33	414.67	0.23	3.37	20.15	39.50	0.99 *[0.97 - 0.99]*	0.99 *[0.99 - 0.99]*
	ESP_B_PM25	5.49	17.89	0.33	3.00	405.00	0.24	3.99	20.56	40.30		
	ESP_C_PM25	5.61	17.79	0.75	3.33	351.75	0.24	4.24	21.58	42.30		
	Ref: IQAIR AVP	3.75	10.81	1.50	3.00	340.40	-	-	-	-		
Temp (°C) BME280	ESP_A_TEMP	24.86	0.73	24.80	25.51	26.63	0.97	3.64	0.16	0.31	0.75 *[0.08 - 0.91]*	0.98 *[0.98 - 0.99]*
	ESP_B_TEMP	25.50	0.87	25.47	26.29	27.44	0.94	4.30	0.29	0.57		
	ESP_C_TEMP	24.59	0.79	24.57	25.29	26.39	0.96	3.39	0.21	0.40		
	Ref: MX1104	21.22	0.70	21.20	21.83	22.88	-	-	-	-		
RH (%) BME280	ESP_A_RH	37.13	3.75	37.35	39.83	50.94	0.99	-10.84	1.14	2.24	0.89 *[0.19 - 0.97]*	1.00 *[1.0 - 1.0]*
	ESP_B_RH	36.32	3.58	36.51	39.01	49.74	0.98	-11.67	1.42	1.42		
	ESP_B_RH	39.22	3.85	39.38	42.05	54.13	0.99	-8.78	1.10	2.16		
	Ref: MX1104	47.93	4.79	48.34	51.44	64.96	-	-	-	-		
Air Prs (hPa) BME280	ESP_A_PRS	992.14	11.81	992.69	1003.36	1011.06	1.00	-4.13	0.45	0.88	1.00 *[0.94 - 1.0]*	1.00 *[1.0 - 1.0]*
	ESP_A_PRS	991.97	11.84	992.48	1003.20	1010.97	1.00	-4.30	0.43	0.85		
	ESP_A_PRS	992.95	11.81	993.51	1004.12	1011.90	1.00	-3.32	0.45	0.89		
	Ref: Weather API	996.25	12.03	996.37	1007.27	1015.19	-	-	-	-		
Light (lux) BH1750	ESP_A_LUX	11.07	23.79	0.00	15.00	294.00	0.95	-4.29	6.04	11.84	0.98 *[0.91 - 0.99]*	0.99 *[0.99 - 0.99]*
	ESP_C_LUX	13.39	23.97	3.00	18.00	300.50	0.95	-1.92	5.59	10.96		
	ESP_C_LUX	8.15	21.86	0.00	9.00	275.25	0.93	-7.71	8.08	15.83		
	Ref: MX1104	14.45	25.88	4.31	22.04	269.84	-	-	-	-		
Noise (dB SPL) INMP441	ESP_A_SOUND	45.17	8.86	42.49	51.57	92.01	0.51	-1.48	6.49	6.49	0.73 *[0.68 - 0.77]*	0.73 *[0.69 - 0.78]*
	ESP_B_SOUND	46.63	8.21	44.00	52.17	84.49	0.49	0.04	6.65	13.04		
	ESP_C_SOUND	45.07	9.33	42.76	52.13	85.66	0.51	-1.05	7.81	15.31		
	Ref: HHSL_101	45.42	5.82	43.20	47.30	102.90	-	-	-	-		

† **Device:** Ref = reference device, ESP_{device}_{Measure} labels refer to the labels used in the dataset to identify multimodal devices; ‡ **Limit of Agreement:** from Bland-Altman analysis; **§ ICCs:** reported with 95% Confidence Intervals that are displayed as *[Lower – Upper]* bounds. The bounds define a range where there is a 1 in 20 chance the true mean should exist. Thus, wider ranges or a low upper-bound indicates a lower reliability.

(resampling, missing data removal, Pearson correlation statistics and data aggregation). The Seaborn library was used in conjunction with Matplotlib to create plots and visualisations and, finally, Sci-Kit Learn, Pingouin and the Stats Models API performed agreement analysis (Intraclass Correlation Coefficients (ICCs), and Bland-Altman) on bivariate pairs.

Correlation and agreement (absolute and consistency) of each low-cost sensor was validated against reference devices. ICC estimates and their 95% confidence intervals were calculated using the Pingouin v0.3.9 [88] library for Python. ICCs were used to assess the reliability of sensor data taken from low-cost sensors against reference devices [89]. Predefined acceptance ratings for ICC were: excellent (>0.900), good (0.750–0.899), moderate (0.500–0.749) and poor (<0.500) [89]–[91].

The Two-Way Random-Effects Model, against a single rater ($ICC_{2,1}$), was used to determine the reliability of randomly chosen low-cost sensors [90]. In this model, the low-cost sensors were evaluated to test the absolute agreement between measurements from each low-cost sensor against the reference device/sensor. This model can be used to generalise findings and evaluate the potential reliability of other sensors (from the same manufacturer) [90]. For example, here we selected three low-cost BH1750 light sensors, and can use $ICC_{2,1}$ to determine the potential reliability of other BH1750 sensors.

The Two-Way Mixed-Effects Model, against a single rater ($ICC_{3,1}$), was used to assess the reliability of this specific sample of sensors [90]. In this model, the consistency of each low-cost sensor is evaluated against a reference. Since this model focuses specifically on the sampled low-cost sensors, the results cannot be generalised to other similar low-cost sensors, even if they share the same characteristics [90]. For example, the consistency of the three BH1750 sensors can be evaluated, but the results cannot be used to determine the consistency of other BH1750 sensors.

Data visualisation

To improve clarity of bivariate visualisations, datasets were resampled to a 1-hour frequency before plots were generated, Figure 3. Bivariate line plots and regression plots were generated to visually inspect data pairs. Finally, the Statsmodel API was used to calculate the mean difference statistics for each data pair. These mean differences were then plotted to Bland-Altman plots, using the Statsmodel Graphic Utilities, to quantify agreement between each data pair [92].

5.3 Sensor deployment

All devices (low-cost multimodal and reference) were placed next to each other on a *(165cm high)* shelf within an office, above a computer desk *(Figure 4).* The office *(located in Newcastle Upon Tyne, UK)* was a south-facing shared office, occupied by two people. Occupants had control over the windows, blinds and heating and the core operating hours were typically between 8am-6pm, Monday to Friday. The position of the shelf meant that no direct light from computer monitors was able to enter the light sensors, so light captured was a mixture of natural daylight and ambient artificial lighting from LED bulbs. Except for the reference sound level meter (Omega HHSL-101), all devices logged sensor readings continuously between 1st – 30th of November 2020. However, the storage capacity of the HHSL-101 meant that data were downloaded, and the sensors reconfigured every three days.

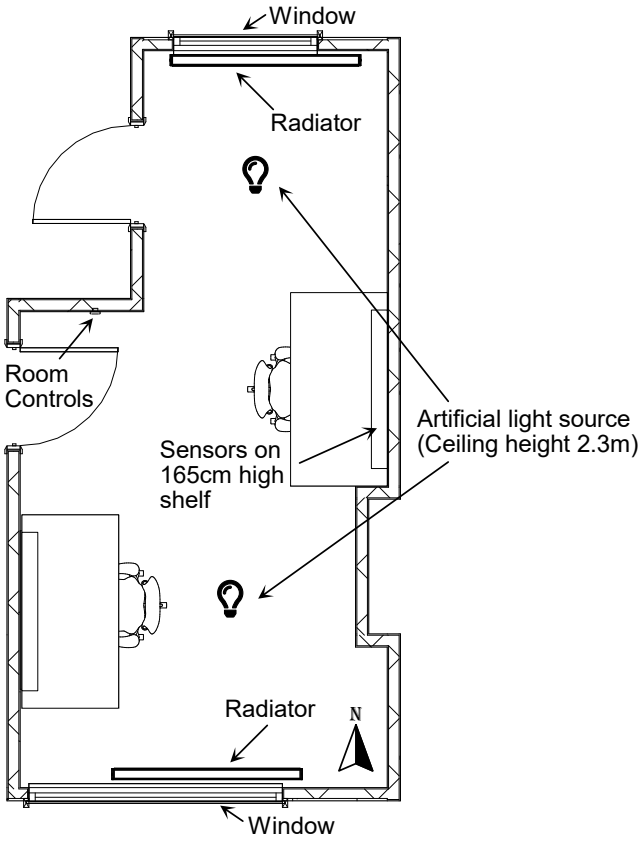

Figure 4 - Layout of office showing placement of windows, doors, artificial light sources and radiators.

5.4 Reference standard setup

All reference standard equipment stored data locally and data were downloaded at the end of the study via the proprietary interfaces. Both HOBO® devices recorded from each of their internal sensors every 5min and stored data internally. Data were then downloaded using the HOBOMobile app.

The AirVisual Pro provides a Server Message Block (SMB) interface. This allows a user to connect to the device, via an IP address, to obtain the stored data files, which are stored in .CSV format. The device has the capability of storing data in the Cloud that can be accessed using the IQAir dashboard. However, to obtain data from the Cloud, a paid subscription is required.

The HHSL-101 also requires use of an application (Omega's Sound DataLogger) to initialise, record and download data. However, this application is only available for Microsoft Windows (XP or greater). The sample rate for the HHSL-101 was set to 10s. From options available, that was the closest to the sample rate of the low-cost multimodal device. At the chosen sample rate, the HHSL-101 was able to capture data for three days only. Therefore, multiple sample periods from this device were conducted throughout November 2020.

6 Results

Due to the number of sensors being evaluated, it is not possible to provide a complete set of data and visualisations. Consequently, a summary of data is presented (Table 4) while data and visualisations used to inform the analysis are included in the online supplementary material.

6.1 Equivalent carbon dioxide (eCO_2)

The MOX eCO_2 sensors had a poor correlation with the reference (≤0.38) and divergence between measurements can be seen across all percentiles, Table 4. When approaching the upper limits of measurements, the measured values are approx. 7000ppm greater than the reference CO_2. There is also little commonality across the mean values and the standard deviations are significantly large. Despite the significant difference in reported values, the MOx sensor data did mostly rise and fall at the same time as the CO_2 reference sensor (Figure 5).

$ICC_{2,1}$ were good (0.79) with broad confidence intervals (0.41 difference between lower and upper bounds). $ICC_{3,1}$ were also good (0.89) but with much narrower confidence intervals (0.01 difference). However, eCO2 sensors had significantly large mean differences against reference CO2 sensors and had and had a larger LoA *(between 350-900ppm)* than the NDIR CO_2 sensors.

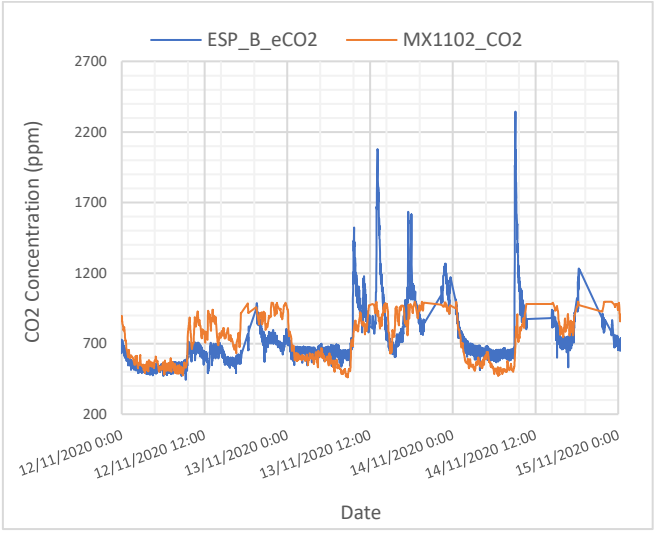

Figure 5 – Snapshot of eCO_2 vs CO_2 events captured by CCS811 (blue) and MX1102 (orange)

6.2 Carbon dioxide (CO_2)

CO_2 measurements across all low-cost sensors were found to strongly correlate with reference data (≥0.95). Low-cost CO_2 sensors appear to generally agree across the lower percentiles but diverge above the 75th percentile. NDIR CO_2 sensor data were closer to the reference data than eCO_2 sensors and had a similar precision to the reference (Figure 6).

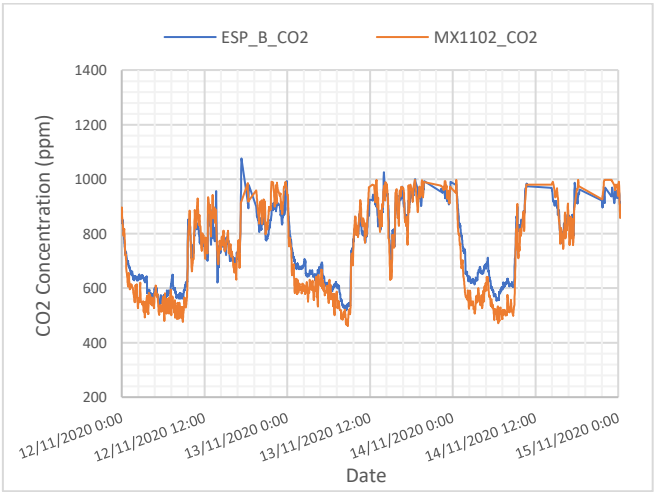

Figure 6 – Snapshot of MH-Z19B CO_2 sensor (blue) vs reference MX1102 CO_2 sensor (orange)

$ICC_{2,1}$ were moderate (0.72), but the confidence intervals were broad (0.8 difference between lower and upper bounds) indicating that other sensors of the same manufacturer and model may have a higher variability than the sensors sampled here. Contrastingly, $ICC_{3,1}$ were excellent (0.95), with a high and narrow confidence interval (0.1 difference between lower and upper bounds). However, the Limit of Agreements (LoAs) were large across all low-cost devices. That notwithstanding, all CO_2 sensors *(including the reference)* have a high standard deviation *(between 132 - 186)*, which may have impacted the LoA.

6.3 Particulate matter

Low-cost $PM_{2.5}$ were found to have poor correlations (≤0.38) to the reference standard. However, there was little divergence across the percentiles. Despite the low Pearson correlations, the low-cost sensors had excellent ICCs for both $ICC_{2,1}$ and $ICC_{3,1}$ (both 0.99). There was also very narrow range between the lower and upper bounds of the confidence intervals (>0.02). This indicates that that there is good inter-sensor reliability.

There was a significantly low mean difference *(between 2 – 4)*, but relatively high LoAs were seen across the low-cost sensors *(≥35µg/m³ more than the reference mean)*. However, the Bland-Altman analysis (Figure 7) highlights that there is a significantly strong agreement between the low-cost and reference sensors during events where dust concentrations are lower. As the dust concentrations increase, the agreement between sensors is reduced, which is likely causing the low correlations. While low-cost $PM_{2.5}$ monitoring devices are considered effective indicators of $PM_{2.5}$ events [48], it is possible that the optical technology used in low-cost $PM_{2.5}$ is not suitable for accurately determining higher concentrations of particulate matter. However, for longitudinal monitoring of IEQ, optical sensors could provide a fit-for-purpose indicator of $PM_{2.5}$ events despite not being able to accurately report values when concentrations exceed around 15µg/m³.

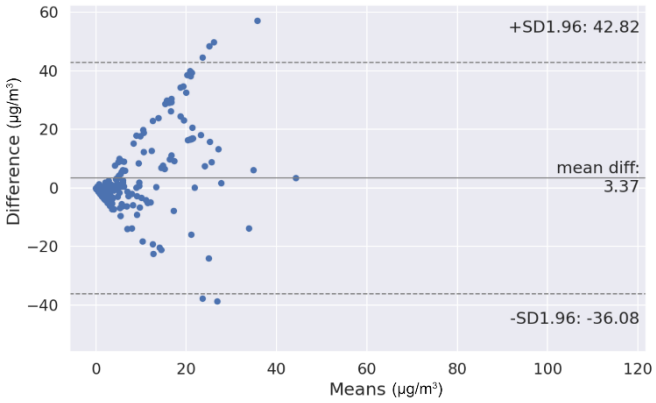

Figure 7 – Bland-Altman plot of PMSA003i means against the Air Visual Pro

6.4 Temperature, humidity (and air pressure)

The multimodal sensor for measuring temperature, relative humidity and air pressure performed well across all measurement factors and were found to have significantly high correlations with the selected reference (≥0.94). While the mean values measured by low-cost sensors did not exactly match the reference means, the values did not diverge through the percentiles and measured with consistent precision *(around 3-4°C mean difference, Figure 8).*

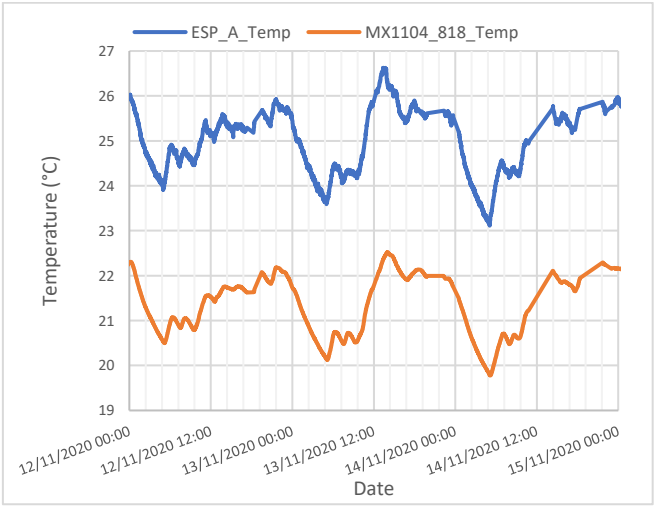

Figure 8 – Comparison of low-cost BME280 temperature sensor (blue) against MX1104 reference (orange).

Like CO_2, the $ICC_{2,1}$ for temperature were good (0.75), but with broad confidence intervals (0.83 difference between lower and upper bounds). However, $ICC_{3,1}$ values indicate excellent reliability among the sample (0.9), with 0.01 difference between the confidence bounds. The BME280 also had the lowest observed LoAs (≤2.3) across all the evaluated sensors.

6.5 Light

Light sensors also performed well against the reference. Low-cost sensors performed consistently across the percentiles and had significant correlations (≥0.93). Mean values and standard deviations agreed with the reference device. Although mean values for light-intensity were lower than expected, it is noted that office users had control over the blinds so were able to mitigate glare (and as such control light intensity) from south-facing windows.

Light sensors were excellent for both $ICC_{2,1}$ (0.98) and $ICC_{3,1}$ (0.99), with high, narrow confidence intervals for both, (≥0.90 with ≤0.08 difference across the lower and upper bounds). This suggests that other sensors of the same manufacturer and model should have similarly low variability across devices.

6.6 Noise

The correlation of noise sensors was approx. 0.50, mildly significant. However, the descriptive statistics agreed with the reference device.

LoAs were also found to be relatively low (≤15.5dB) and the ICCs for both $ICC_{2,1}$ and $ICC_{3,1}$ showed moderate reliability (0.73), with only 0.09 difference between the lower and upper bounds for both ICCs. This indicates good inter-sensor reliability. The sensors also performed consistently across all percentiles showing the lowest recorded mean difference against the reference (≤1.48).

7 Discussion

This study proposed and developed a multimodal IEQ monitoring device to achieve scalable and individualised IEQ monitoring. A background of related work was presented to identify a range of sensors and technologies used to construct and configure a low-cost, IoT enabled device. A detailed analytical study compared variations across low-cost sensors and a comparison to reference standards.

7.1 MEMS sensor selection

Use of I^2C MEMS sensors meant that fewer General-Purpose Inputs/Outputs (GPIOs) were required on the microcontroller. As a result, smaller microcontrollers with less GPIOs could be used. Moreover, selected MEMS sensors had integrated ADCs negating the requirement for a microcontroller with a high resolution ADC, which can be more costly [1]. Also, using a digital I^2S MEMS microphone meant that the proximity with WiFi and Bluetooth components *(required by a small form-factor, multimodal, IoT device)* would not interfere with the microphone's performance.

Use of MEMS sensors did identify certain drawbacks. For example, many MEMS sensors *(e.g., CCS811, BH1750, BME280)* have built-in controllers that enable the ADC conversions and signal processing. However, this can often result in a sensor that performs 'hidden', black boxed algorithms on data, which can be problematic in research settings where transparency is key. Understanding, *e.g.*, how the CCS811 calculates TVOC and eCO_2 could be beneficial to researchers and help to better assess calculation validity or to develop algorithms against the unreported raw data.

7.2 Sensor performance

$ICC_{2,1}$ indicated good-to-excellent reliability for all sensors. However, the range between lower and upper bounds of the 95% confidence intervals was as much greater in some cases *(CO_2: 0.9; Temperature: 0.83).* This indicates that the sensors sampled here cannot be used to determine the reliability of other sensors with the same characteristics.

Most sensors however *(MH-Z19, PMSA003i, BME280, BH1750)* had excellent $ICC_{3,1}$ (≥0.95) with a 95% confidence range of 0.01 between the upper and lower bounds. This indicates that this sample of sensors had excellent inter-sensor reliability. The sound and eCO_2 sensors did not perform as well, but $ICC_{3,1}$ were still good (0.89) with a 95% confidence range of 0.01 between the upper and lower bounds.

Accuracy and precision

This study confirmed findings [3] that low-cost sensors can often have high precision, but with a reduced accuracy. A clear misalignment between the two datasets (i.e., low accuracy) was found, but the low-cost sensor responded with the same precision as the reference. This was not the case for all sensors, but CO2, Temperature, Relative Humidity, Air Pressure and Light all had high precision.

Due to the high precision, it is possible to calibrate the devices against the mean difference between the low-cost sensor and the reference. However, since light intensity dropped to 0lx at night, adjusting against the mean difference alone would result in negative values, so measurement ranges need to be considered when calibrating sensors.

7.3 Ventilation sensors for air quality

Here, MOx eCO_2 sensor data was erratic, when compared against actual CO_2 measurements. Reported values from the MOx sensors did mostly rise and fall at the time as the CO_2 reference sensor, but the reported values for eCO_2 were often far greater than the reference. Since MOx sensors are highly sensitive to a range of environmental factors [22], It is possible that these sensors are responding to the accumulation of unventilated air *(as opposed to actual CO_2).* In this way, they may be useful as proxies for ventilation measurement in the same way CO_2 sensors are used [37], [38].

More research is required to assess whether eCO_2/TVOC sensors are fit-for-purpose in ventilation monitoring. However, they could provide an affordable and scalable solution *(compared to NDIR CO_2 sensors)* to address the growing need for ventilation monitoring brought on by the SARS-COV-2 pandemic. Therefore, there are strong practical implications for identifying eCO_2/TVOC sensors as proxies for ventilation.

If eCO_2 sensors are found to be suitable for indoor ventilation monitoring, it would be preferable to report data from these sensors with more appropriate terminology, as the eCO_2 terminology implies the measurement is related to carbon dioxide, which cannot be confirmed by this study.

7.4 Cloud connectivity

The use of ThingSpeak® in this study was beneficial as it provided an IoT platform to capture data in real-time, without needing to connect to devices or download data from internal storages. This was advantageous as it meant a sample could be downloaded during the data collection phase and used to develop code needed for analysis, reducing the workload at the end of the project. ThingSpeak® also allowed for real-time monitoring of the data, providing graphs and visualisations. While the platform was previously deemed currently unsuitable for real-time medical monitoring [1], this study confirmed that it is suitable for prototyping/small scale IEQ monitoring projects. The platform is also scalable and provides a clear pricing calculator so project costs can be easily projected. However, the quota strategies used by larger Cloud computing platforms *(e.g., Amazon Web Services)* may be better suited for larger projects as resources can be shared and distributed amongst multiple devices more easily [1]. It is also worth noting that the IoT cloud platform market is rapidly growing and there are more than 600 dedicated platforms available, each designed with nuanced use-cases [1], [74]. It is recognised here that while ThingSpeak® was suitable for this study, the quotas and limitations it imposes may create a requirement for researchers to conduct an analysis of the IoT platform market to assess available platforms.

7.5 Limitations

Only three low-cost multimodal devices were examined in this study. With more resources, more devices could have been examined, which would have provided a greater sample size for ICC analyses. While three sensors is enough to conduct a reliability study, a greater number of sensors would reduce the potential lack of variability between sensors, which may impact ICC estimations [90].

All devices were connected to a premium residential network package (Virgin Media, Reading, UK). However, on occasions during the study period the internet was heavily interrupted, which caused the devices to disconnect and resulted in lost data. Regardless, there was ample data to conduct an informed analysis and comparison of all sensors.

The measurement ranges captured by sensors in this study were measured under normal operating conditions so there was no necessity to test the upper/lower limits of the sensors (i.e. at extreme conditions). Therefore, it was not possible to evaluate the LoA for sensors in those ranges. Nevertheless, Bland-Altman analyses did highlight *(for sensors that approached upper office comfort limits)* that LoAs did diverge as values increased (Figure 7). Researchers wishing to use these sensors under more extreme conditions should be mindful of this and further evaluate the sensors under the desired measurement conditions.

7.6 Future Work

The affordability and multimodality of the device proposed here identifies a scalable solution for occupant monitoring that can provide a guidance around IEQ in buildings. Future work should exploit the affordability of these sensors to deploy multimodal devices for longer periods of time (i.e. continuously) and address the needs for localised monitoring of building occupants, by deploying sensors at an individual level to understand the IEQ variability in multi-occupant spaces. This could be beneficial to understanding health and wellbeing of building occupants, but it could also add more spatial density to environmental monitoring, which could have pragmatic implications to the operation of buildings. For example, building management systems could make use of the spatially dense data captured from localised monitoring solutions, which could be used to inform the operation, and evaluate the performance of e.g., HVAC systems and other building services. Future work should also aim to identify calibration offsets that can be applied to individual measurement factors to account for poor accuracy and to ensure the validity of sensors using determined offsets.

8 Conclusions

Sensors used in this study would be suitable for continuous monitoring to provide building occupants with an indication of environmental quality and changes. Despite inaccuracies in certain sensors, the high precision witnessed means that

in most cases the sensors can be calibrated easily against the mean differences recorded in this study. However, the $ICC_{2,1}$ showed that the variability of sensors seen in this study may not be representative of other sensors with the same make/model. Therefore, with the findings from this study alone, it would not be possible to provide a general calibration offset that would be applicable for other sensors.

In certain cases, it may be preferable to report data from sensors as a red/amber/green system instead of using the numerical output. For example, eCO2 was found to be unsuitable as a measurement of carbon dioxide but showed potential as a proxy measure for ventilation. While further research would be needed to confirm this, reporting data as Parts Per Million, the unit of measurement for CO_2, may not be applicable for this application.

Given the potential accuracy biases found in this study, it would not be possible to ensure the scientific validity of the sensors for use in applications such as occupational health assessments or standard compliance. However, the intended use-case for the devices proposed here is to provide building occupants with a general indication of environmental changes. For this application, this study found evidence that the specific sensors sampled in this study are fit-for-purpose. Consequently, the multimodal device developed here could provide a viable solution for localised, continuous monitoring that could be pragmatically deployed at scale.

9 Data

Additional data and visualisations used in this study are available via online supplementary material.

10 Funding

This work was supported by the European Regional Development Intensive Industrial Innovation Programme (IIIP) as part of doctoral research, Grant Number: 25R17P01847. The sponsoring small to medium enterprise for this programme was Ryder Architecture and it was delivered through Northumbria University.

11 References

[1] G. Coulby, A. Clear, O. Jones, and A. Godfrey, "Towards remote healthcare monitoring using accessible IoT technology: State-of-the-art, insights and experimental design," *Biomed. Eng. Online*, 2020.

[2] Well Building Institute, "WELL Building Standard ® v1 Copyright," 2019. https://www.wellcertified.com/en/system/files/WELL v1 with 2018 Q4 Addenda.pdf (accessed Mar. 08, 2019).

[3] G. Coulby, A. Clear, O. Jones, and A. Godfrey, "A Scoping Review of Technological Approaches to Environmental Monitoring," *Int. J. Environ. Res. Public Heal. 2020, Vol. 17, Page 3995*, vol. 17, no. 11, p. 3995, Jun. 2020, doi: 10.3390/IJERPH17113995.

[4] A. Godfrey, M. Brodie, K. S. van Schooten, M. Nouredanesh, S. Stuart, and L. Robinson, "Inertial wearables as pragmatic tools in dementia," *Maturitas*, vol. 127, no. May, pp. 12–17, 2019, doi: 10.1016/j.maturitas.2019.05.010.

[5] X. Shan, J. Zhou, V. W. C. Chang, and E. H. Yang, "Comparing mixing and displacement ventilation in tutorial rooms: Students' thermal comfort, sick building syndromes, and short-term performance," *Build. Environ.*, vol. 102, pp. 128–137, Jun. 2016, doi: 10.1016/j.buildenv.2016.03.025.

[6] Y. Tang, C. Shrubsole, and H. Altamirano, "Indoor Air Quality and Thermal Comfort: is all well with the Well Standard?'," 2017, Accessed: Jul. 29, 2018. [Online]. Available: http://discovery.ucl.ac.uk/1574715/1/MC2017_Tang_Yarong.pdf.

[7] N. Clements *et al.*, "The Spatial and Temporal Variability of the Indoor Environmental Quality during Three Simulated Office Studies at a Living Lab," *Buildings*, vol. 9, no. 3, p. 62, Mar. 2019, doi: 10.3390/buildings9030062.

[8] S. Mcdonald and D. W. Johnston, "Exploring the contributions of n-of-1 methods to health psychology research and practice," *Heal. Psychol. Updat.*, vol. 28, pp. 38–40, 2019, Accessed: Mar. 27, 2019. [Online]. Available: https://www.researchgate.net/publication/331639838.

[9] A. Moreno-Rangel, T. Sharpe, F. Musau, and G. McGill, "Field evaluation of a low-cost indoor air quality monitor to quantify exposure to pollutants in residential environments," *J. Sensors Sens. Syst.*, vol. 7, no. 1, pp. 373–388, 2018, doi: 10.5194/jsss-7-373-2018.

[10] K. C. Coombs *et al.*, "Indoor air quality in green-renovated vs. non-green low-income homes of children living in a temperate region of US (Ohio)," *Sci. Total Environ.*, vol. 554–555, pp. 178–185, 2016, doi: 10.1016/j.scitotenv.2016.02.136.

[11] Y. Hua, Ö. Göçer, and K. Göçer, "Spatial mapping of occupant satisfaction and indoor environment quality in a LEED platinum campus building," *Build. Environ.*, vol. 79, pp. 124–137, 2014, doi: 10.1016/j.buildenv.2014.04.029.

[12] V. Földváry, G. Bekö, S. Langer, K. Arrhenius, and D. Petráš, "Effect of energy renovation on indoor air quality in multifamily residential buildings in Slovakia," *Build. Environ.*, vol. 122, pp. 363–372, 2017, doi: 10.1016/j.buildenv.2017.06.009.

[13] K. W. Mui, L. T. Wong, H. C. Yu, and T. W. Tsang, "Development of a user-friendly indoor environmental quality (IEQ) calculator in air-conditioned offices," *IAQVEC 2016 - 9th Int. Conf. Indoor Air Qual. Vent. Energy Conserv. Build.*, no. June 2017, 2016.

[14] Andargie MS; Touchie M; O'Brien W, "A review of factors affecting occupant comfort in multi-unit residential buildings," *Build. Environ.*, vol. 160, no. April, p. 106182, 2019, doi: 10.1016/J.BUILDENV.2019.106182.

[15] Y. Al horr, M. Arif, M. Katafygiotou, A. Mazroei, A. Kaushik, and E. Elsarrag, "Impact of indoor environmental quality on occupant well-being and comfort: A review of the literature," *Int. J. Sustain. Built Environ.*, vol. 5, no. 1, pp. 1–11, Jun. 2016, doi: 10.1016/j.ijsbe.2016.03.006.

[16] Arduino, "Arduino Library List - Arduino Libraries," 2020. https://www.arduinolibraries.info/ (accessed Apr. 22, 2020).

[17] J. Kwon, G. Ahn, G. Kim, J. C. Kim, and H. Kim, "A Study on NDIR-based CO2 Sensor to apply Remote Air Quality Monitoring System," *2009 ICCAS-SICE*, pp. 1683–1687, 2009.

[18] S. Chen and Q. Chen, "Self-Regulation and Parameters Monitoring System for Culturing Chamber," *2018 4th Int. Conf. Comput. Commun. Autom.*, pp. 1–6, 2019, doi: 10.1109/ccaa.2018.8777716.

[19] S. S. Chiang, C. H. Huang, and K. C. Chang, "A minimum hop routing protocol for home security systems using wireless sensor networks," *IEEE Trans. Consum. Electron.*, vol. 53, no. 4, pp. 1483–1489, 2007, doi: 10.1109/TCE.2007.4429241.

[20] J. Saini, "Internet of Things Based Environment Monitoring and PM 10 Prediction for Smart Home," 2020.

[21] P. T. Moseley, "Solid state gas sensors," 1997.

[22] R. Piedrahita *et al.*, "Article in Atmospheric Measurement Techniques · February," *Atmos. Meas. Tech*, vol. 7, pp. 3325–3336, 2014, doi: 10.5194/amtd-7-2425-2014.

[23] J. W. Bennett and A. A. Inamdar, "Are some fungal volatile organic compounds (VOCs) mycotoxins?," *Toxins*, vol. 7, no. 9. MDPI AG, pp. 3785–3804, Sep. 22, 2015, doi: 10.3390/toxins7093785.

[24] AMS, "CCS811 Datasheet," 2016. http://ams.com/eng/Products/Environmental-Sensors/Air-Quality-Sensors/CCS811 (accessed Aug. 28, 2019).

[25] AMS, "iAQ-Core Datasheet," 2016. https://www.mouser.co.uk/datasheet/2/588/iAQ-core_DS000334_1-00-1512544.pdf (accessed Aug. 28, 2019).

[26] Sensortech, “MiCS-VZ-89TE Data sheet.” https://sgx.cdistore.com/datasheets/e2v/MiCS-VZ-89TE_V1.0.pdf (accessed Aug. 28, 2019).
[27] F. Naepelt, R. Schreiber, M. Groening, and C. Meyer, “An Indoor Air Quality System for IoT applications,” *Sensoren und Messsyst. - 19. ITG/GMA-Fachtagung*, pp. 581–584, 2018.
[28] I. Siti Hamimah, D. Baba, and L. Abd Mutalib, “Indoor Air Quality Issues for Non-Industrial Work Place,” 2010. Accessed: Mar. 14, 2019. [Online]. Available: https://pdfs.semanticscholar.org/af92/0a14d9f68a1eaaa2f77571c980f453abc2e7.pdf.
[29] G. Guyot, M. H. Sherman, and I. S. Walker, “Smart ventilation energy and indoor air quality performance in residential buildings: A review,” *Energy Build.*, vol. 165, pp. 416–430, Apr. 2018, doi: 10.1016/J.ENBUILD.2017.12.051.
[30] A. Rusu and P. Dobra, “Using adaptive transmit power in wireless indoor air quality monitoring,” *2019 23rd Int. Conf. Syst. Theory, Control Comput. ICSTCC 2019 - Proc.*, pp. 543–548, 2019, doi: 10.1109/ICSTCC.2019.8885849.
[31] Y. Yang, “Design and Application of Intelligent Agriculture Service System with LoRa-based on Wireless Sensor Network,” *Proc. - 2020 Int. Conf. Comput. Eng. Appl. ICCEA 2020*, pp. 712–716, 2020, doi: 10.1109/ICCEA50009.2020.00155.
[32] S. Kulkarni, N. G. Kalayil, J. James, S. Parsewar, and R. Shriram, “Detection of Parkinson’s Disease through Smell Signatures,” *Proc. 2020 IEEE Int. Conf. Commun. Signal Process. ICCSP 2020*, vol. 411052, pp. 808–812, 2020, doi: 10.1109/ICCSP48568.2020.9182283.
[33] Adafruit, “adafruit/Adafruit_CCS811: Arduino driver for CCS811 digital gas sensor,” 2021. https://github.com/adafruit/Adafruit_CCS811 (accessed Feb. 01, 2021).
[34] J. G. Allen, P. MacNaughton, U. Satish, S. Santanam, J. Vallarino, and J. D. Spengler, “Associations of cognitive function scores with carbon dioxide, ventilation, and volatile organic compound exposures in office workers: A controlled exposure study of green and conventional office environments,” *Environ. Health Perspect.*, 2016, doi: 10.1289/ehp.1510037.
[35] T. Parkinson, A. Parkinson, and R. de Dear, “Continuous IEQ monitoring system: Performance specifications and thermal comfort classification,” *Build. Environ.*, vol. 149, no. February, pp. 241–252, 2019, doi: 10.1016/j.buildenv.2018.12.016.
[36] J. R. Coleman and F. Meggers, “Sensing of Indoor Air Quality—Characterization of Spatial and Temporal Pollutant Evolution Through Distributed Sensing,” *Front. Built Environ.*, vol. 4, p. 28, Aug. 2018, doi: 10.3389/fbuil.2018.00028.
[37] J. M. Daisey, W. J. Angell, and M. G. Apte, “Indoor air quality, ventilation and health symptoms in schools: an analysis of existing information.,” *Indoor Air*, vol. 13, no. 1, pp. 53–64, 2003, [Online]. Available: http://www.ncbi.nlm.nih.gov/pubmed/12608926.
[38] K. Rogage, A. Clear, Z. Alwan, T. Lawrence, and G. Kelly, “Assessing Building Performance in Residential Buildings using BIM and Sensor Data,” *Int. J. Build. Pathol. Adapt.*, 2019, doi: 10.1108/IJBPA-01-2019-0012.
[39] M. Freiburg, “CO2 measurements in instrumental and vocal closed room settings as a risk reducing measure for a Coronavirus infection b,” 2020.
[40] Umwelt-Campus, “COVID-19 prevention: CO2 measurement and demand.” https://www.umwelt-campus.de/forschung/projekte/iot-werkstatt/ideen-zur-corona-krise (accessed Jan. 22, 2021).
[41] F. H. L. Koppens, T. Mueller, P. Avouris, A. C. Ferrari, M. S. Vitiello, and M. Polini, “Photodetectors based on graphene, other two-dimensional materials and hybrid systems,” *Nat. Nanotechnol.*, vol. 9, no. 10, pp. 780–793, 2014, doi: 10.1038/nnano.2014.215.
[42] A. Martín-Garín, J. A. Millán-García, A. Baïri, J. Millán-Medel, and J. M. Sala-Lizarraga, “Environmental monitoring system based on an Open Source Platform and the Internet of Things for a building energy retrofit,” *Autom. Constr.*, vol. 87, pp. 201–214, Mar. 2018, doi: 10.1016/j.autcon.2017.12.017.
[43] G. Marques, C. R. Ferreira, and R. Pitarma, “Indoor Air Quality Assessment Using a CO 2 Monitoring System Based on Internet of Things,” *J. Med. Syst.*, vol. 43, no. 3, 2019, doi: 10.1007/s10916-019-1184-x.
[44] H. Nijzink, “A Homemade Air Quality Sensor: Is it viable?,” Bachelor’s thesis, University of Twente, 2018.
[45] J. Dempsey, “WifWaf/MH-Z19: For Arduino Boards (&ESP32). Additional Examples/Commands., Hardware/Software Serial,” *Github*, 2021. https://github.com/WifWaf/MH-Z19 (accessed Feb. 01, 2021).
[46] S. C. Lee *et al.*, “PM1.0 and PM2.5 characteristics in the roadside environment of Hong Kong,” *Aerosol Sci. Technol.*, vol. 40, no. 3, pp. 157–165, 2006, doi: 10.1080/02786820500494544.
[47] Environmental Protection Agency, “National Ambient Air Quality Standards for Particulate Matter; Final Rule,” *Fed. Regist.*, vol. 78, no. 10, pp. 3086–3287, 2013.
[48] Z. Wang, W. W. Delp, and B. C. Singer, “Performance of low-cost indoor air quality monitors for PM2.5 and PM10 from residential sources,” *Build. Environ.*, vol. 171, p. 106654, Mar. 2020, doi: 10.1016/j.buildenv.2020.106654.
[49] B. Laquai, “Particle Distribution Dependent Inaccuracy of the Plantower PMS5003 low- cost PM-sensor Particle Distribution Dependent Inaccuracy of the Plantower PMS5003 low- cost PM-sensor,” 2017. [Online]. Available: https://www.researchgate.net/publication/320555036_Particle_Distribution_Dependent_Inaccuracy_of_the_Plantower_PMS5003_low-cost_PM-sensor.
[50] M. Levy Zamora, F. Xiong, D. Gentner, B. Kerkez, J. Kohrman-Glaser, and K. Koehler, “Field and Laboratory Evaluations of the Low-Cost Plantower Particulate Matter Sensor,” *Environ. Sci. Technol.*, vol. 53, no. 2, pp. 838–849, 2019, doi: 10.1021/acs.est.8b05174.
[51] H. Mei *et al.*, “Field evaluation of low-cost particulate matter sensors in Beijing,” *Sensors (Switzerland)*, vol. 20, no. 16, pp. 1–17, 2020, doi: 10.3390/s20164381.
[52] Adafruit, “adafruit/Adafruit_PM25AQI: Arduino library for PMS* Air Quality Sensors,” *Github*, 2021. https://github.com/adafruit/Adafruit_PM25AQI (accessed Feb. 01, 2021).
[53] Y. Liu, X. Ni, Y. Wu, and W. Zhang, “Study on effect of temperature and humidity on the CO2 concentration measurement,” *IOP Conf. Ser. Earth Environ. Sci.*, vol. 81, no. 1, 2017, doi: 10.1088/1755-1315/81/1/012083.
[54] P. Dani, P. Adi, and A. Kitagawa, “Performance Evaluation of E32 Long Range Radio Frequency 915 MHz based on Internet of Things and Micro Sensors Data,” 2019. Accessed: Nov. 16, 2020. [Online]. Available: www.ijacsa.thesai.org.
[55] Adafruit, “adafruit/Adafruit_BME280_Library: Arduino Library for BME280 sensors,” *Github*, 2020. https://github.com/adafruit/Adafruit_BME280_Library (accessed Feb. 01, 2021).
[56] M. J. Jafari and A. Asghar, “Association of Sick Building Syndrome with Indoor Air Parameters,” vol. 14, no. 1, pp. 55–62, 2015.
[57] F. P. Jooste, A. Kumar, and G. P. Hancke, “Energy efficient irrigation scheduling system based on the ISO/IEC/IEEE 21451 standards,” *Proc. IEEE Int. Conf. Ind. Technol.*, pp. 1441–1446, 2017, doi: 10.1109/ICIT.2017.7915577.
[58] L. H. M. de Castro, B. L. Lago, and F. Mondaini, “Damped Harmonic Oscillator with Arduino,” *J. Appl. Math. Phys.*, vol. 03, no. 06, pp. 631–636, 2015, doi: 10.4236/jamp.2015.36075.
[59] L. Sánchez, I. Elicegui, J. Cuesta, L. Muñoz, and J. Lanza, “Integration of Utilities Infrastructures in a Future Internet Enabled Smart City Framework,” *Sensors*, vol. 13, no. 11, pp. 14438–14465, Oct. 2013, doi: 10.3390/s131114438.
[60] PeterEmbedded, “BH1750FVI - Arduino Libraries,” 2018. https://www.arduinolibraries.info/libraries/bh1750-fvi (accessed Apr. 22, 2020).
[61] ELEXHUB, “ELEXHUB Tutorial: BH1750 Digital Light Intensity Sensor,” 2016. Accessed: Feb. 01, 2021. [Online]. Available: http://elexhub.com/wp-content/uploads/2016/10/ELEXHUB-Tutorial_BH1750-Digital-Light-Intensity-Sensor.pdf.
[62] R. Osborne, M. Ward, and K. Dawkins, “A micro-machined acoustic sensor array for fuel level indication,” *Sensors Actuators, A Phys.*, vol. 115, no. 2-3 SPEC. ISS., pp. 385–391, 2004, doi: 10.1016/j.sna.2004.04.044.
[63] G. Balakrishnan, G. Sainarayanan, R. Nagarajan, and S. Yaacob, “A stereo image processing system for visually impaired,” *Int. J. Comput. Electr. Autom. Control Inf. Eng.*, vol. 2, no. 8, pp. 2794–2803, 2008, [Online]. Available: http://waset.org/Publication/a-stereo-image-processing-system-for-visually-impaired/10379.
[64] B. Bank, “Logarithmic frequency scale parallel filter design with complex and magnitude-only specifications,” *IEEE Signal Process. Lett.*, vol. 18, no. 2, pp. 138–141, 2011, doi: 10.1109/LSP.2010.2093892.
[65] J. Lewis and B. Moss, “MEMS Microphones, the Future for Hearing Aids,” *Analog Dialogue*, vol. 47, no. 11, pp. 3–5, 2013.

[66] J. Lewis, “MS-2472: Analog and Digital MEMS Microphone Design Considerations,” pp. 1–4, 2013.
[67] I. Kostoski, “ikostoski/esp32-i2s-slm: Sound Level Meter with ESP32 and I2S MEMS microphone,” *Github*, Nov. 22, 2019. https://github.com/ikostoski/esp32-i2s-slm (accessed Jul. 31, 2020).
[68] Z. Winsen and E. Technology, “Intelligent Infrared CO2 Module (Model: MH-Z19B),” pp. 1–9, 2016.
[69] Z. Yong and Z. Haoxin, “Digital universal particle concentration sensor PMS6003 series data manual Writer,” *Prod. data Man. PLANTOWER*, vol. c, p. 15, 2016, [Online]. Available: https://download.kamami.pl/p564008-PMS7003 series data manua_English_V2.5.pdf.
[70] Bosch Sensortec, “BME280 Combined humidity and pressure sensor,” 2020. Accessed: Apr. 14, 2021. [Online]. Available: https://www.bosch-sensortec.com/media/boschsensortec/downloads/datasheets/bst-bme280-ds002.pdf.
[71] ROHM, “Digital 16bit Serial Output Type Ambient Light Sensor IC BH1750FVI,” 2011. Accessed: Apr. 14, 2021. [Online]. Available: www.rohm.com.
[72] InvenSense, “INMP441 Omnidirectional Microphone with Bottom Port and I 2 S Digital Output,” vol. 1, no. 408, pp. 1–20, 2014.
[73] P. Pierleoni, R. Concetti, A. Belli, and L. Palma, “Amazon, Google and Microsoft Solutions for IoT: Architectures and a Performance Comparison,” *IEEE Access*, vol. 8, pp. 5455–5470, 2020, doi: 10.1109/ACCESS.2019.2961511.
[74] K. L. Lueth, “IoT Platform Companies Landscape 2020,” *IOT Analytics*, 2019. https://iot-analytics.com/iot-platform-companies-landscape-2020/ (accessed Jul. 14, 2020).
[75] T. Collins, “EQuALS – Environmental quality in active learning spaces.”
[76] S. Liu *et al.*, “Predicted percentage dissatisfied with vertical temperature gradient,” *Energy Build.*, vol. 220, 2020, doi: 10.1016/j.enbuild.2020.110085.
[77] D. Licina, Y. Tian, and W. W. Nazaroff, *Experimental investigation of inhalation intake fraction from localized indoor particle sources*. 2017.
[78] M. A. Molina, “Design and development of a methodology to monitor PM10 dust particles produced by industrial activities using UAV’s Sustainable Mineral Institute.”
[79] S. H. Kim *et al.*, “The Impact of Composition in Non-steel and Low-Steel Type Friction Materials on Airborne Brake Wear Particulate Emission,” *Tribol. Lett.*, vol. 68, no. 4, p. 118, Dec. 2020, doi: 10.1007/s11249-020-01361-2.
[80] Onset Computer Corporation, “HOBO® MX CO 2 Logger (MX1102) Manual,” 2017. Accessed: Apr. 14, 2021. [Online]. Available: www.onsetcomp.com.
[81] Onset Computer Corporation, “HOBO MX1104 Data Logger Specifications,” 2021. Accessed: Apr. 14, 2021. [Online]. Available: www.onsetcomp.com/support/contact.
[82] IQAir, “Technical Specifications: AirVisual Pro,” 2021. https://www2.iqair.com/sites/default/files/documents/AVP_TS_NA.pdf (accessed Apr. 14, 2021).
[83] Omega, “Digital Sound Level Data Logger HHSL-101,” 2021. https://br.omega.com/omegaFiles/das/pdf/HHSL-101.pdf (accessed Apr. 14, 2021).
[84] F. Leens, “An introduction to I2C and SPI protocols,” *IEEE Instrumentation and Measurement Magazine*, vol. 12, no. 1, pp. 8–13, 2009.
[85] M. Wu and H. Zhang, “Interface Technology,” vol. 119, no. Icacie, pp. 26–30, 2017.
[86] E. T. Louokdom *et al.*, “Small-scale modular multilevel converter for multi-terminal DC networks applications: System control validation,” *Energies*, vol. 11, no. 7, 2018, doi: 10.3390/en11071690.
[87] V. Jain and R. M. Patrikar, “A Low-Cost Portable Dynamic Droplet Sensing System for Digital Microfluidics Applications,” *IEEE Trans. Instrum. Meas.*, vol. 69, no. 6, pp. 3623–3630, 2020, doi: 10.1109/TIM.2019.2932526.
[88] R. Vallat, “Pingouin: statistics in Python,” *J. Open Source Softw.*, vol. 3, no. 31, p. 1026, Nov. 2018, doi: 10.21105/joss.01026.
[89] P. E. Shrout and J. L. Fleiss, “Intraclass correlations: uses in assessing rater reliability.1. Shrout PE, Fleiss JL: Intraclass correlations: uses in assessing rater reliability. Psychol Bull 1979, 86:420–8.,” *Psychol. Bull.*, vol. 86, no. 2, pp. 420–8, 1979, [Online]. Available: http://www.ncbi.nlm.nih.gov/pubmed/18839484.
[90] T. K. Koo and M. Y. Li, “A Guideline of Selecting and Reporting Intraclass Correlation Coefficients for Reliability Research,” *J. Chiropr. Med.*, vol. 15, no. 2, pp. 155–163, Jun. 2016, doi: 10.1016/j.jcm.2016.02.012.
[91] A. Hartmann, S. Luzi, K. Murer, R. A. de Bie, and E. D. de Bruin, “Concurrent validity of a trunk tri-axial accelerometer system for gait analysis in older adults,” *Gait Posture*, vol. 29, no. 3, pp. 444–448, 2009, doi: 10.1016/j.gaitpost.2008.11.003.
[92] D. Giavarina, “Understanding Bland Altman analysis,” *Biochem. Medica*, vol. 25, no. 2, pp. 141–151, 2015, doi: 10.11613/BM.2015.015.